Seamless Convergence of Fiber and Wireless Systems for 5G and Beyond Networks

Pham Tien Dat ⓘ, *Member, IEEE*, Atsushi Kanno ⓘ, *Member, IEEE*, Naokatsu Yamamoto,
and Tetsuya Kawanishi ⓘ, *Fellow, IEEE*

(Invited Paper)

Abstract—**We propose different fronthaul systems for facilitating future mobile networks based on the seamless convergence of fiber-optic and wireless systems in the millimeter-wave (mmWave) bands. First, a flexible and high-performance wireless fronthaul system is proposed through an encapsulation of radio signals onto a converged fiber–mmWave system. A simultaneous transmission of three radio signals over the system is successfully demonstrated. Second, a high-performance optical self-heterodyne system is proposed and demonstrated for the generation and transmission of radio access signals in high-frequency bands. Third, a high-spectral-efficiency optical fronthaul system for the simultaneous transmission of multiple radio signals in different frequency bands is proposed using a subcarrier-multiplexing intermediate-frequency-over-fiber system. Satisfactory performance is experimentally confirmed for the transmission of three different radio signals in the microwave and low- and high-mmWave bands. The proposed systems can overcome the challenges and bottlenecks of the current mobile fronthaul systems and can be useful in different usage scenarios of 5G and beyond networks.**

Index Terms—**5G and beyond networks, fiber-wireless convergence, mobile fronthaul, radio-over-fiber.**

I. INTRODUCTION

RECENTLY, ITU-R and 3GPP have defined main use cases for 5G and beyond networks, in which the main 5G features comprise enhanced mobile broadband (eMBB), massive type communications (mMTC), and ultra-reliable and low-latency communications (uRLLC) [1], [2]. At the ITU-R, these three features are considered the key usage scenarios of the IMT-2020 system. At the 3GPP, the main requirements for 5G new radios (NRs) for each usage scenario have been determined. For the eMBB use case, the peak data rates of 20 Gbps and 10 Gbps have been set in the downlink and uplink, respectively. The

use of high carrier frequencies and carrier aggregation spanning multiple bands is also anticipated. The key performance indicators for the mMTC usage are to increase the connection density and expand the coverage to support the spread of internet of things (IoT). For the uRLLC use case, a very low latency of 0.5 μs has been set as a target value. For radio access networks (RANs), frequency bands below 6 GHz will be used for the evolution of long-term evolution-advanced (LTE-A) and LTE-A Pro, such as Release 15 and beyond, with the enhancement to machine type communication or narrow-band-IoTs. New frequency bands below 6 GHz can also be used for new waveforms and NRs with ultra-dense small cells and wireless local access networks. Some pre-5G standards, such as Verizon wireless [3], operate primarily in the 28 GHz band. In other NRs, frequencies from 30 to 40 GHz are expected to be mainly utilized. For example, the United States has defined 27.5–28.35 GHz, together with the 38.6–40 GHz and 37–38.6 GHz bands, as their spectrum frontier bands. Japan has defined the 27.5–29.5 GHz band as a candidate for 5G and planned to provide 5G services during 2020 Tokyo Olympic Games [4]. For new RANs beyond 2020, frequency bands up to 100 GHz or higher are considered potential candidates for achieving the target increase of 1000 times in the throughput to end users. Together with the use of high-frequency RANs, other advanced technologies, such as massive multiple-input multiple-output (MIMO) and beamforming, will be employed to overcome the propagation loss of radio signals in high-frequency bands [5].

The evolution of RANs in 5G and beyond networks with stringent requirements on data rate, latency, and density will pose significant challenges to the transport networks, especially to the fronthaul systems for transporting radio signals from a cloud to antenna sites. Recently, a next-generation fronthaul interface (NGFI) has been proposed for reducing the required data rate of fronthaul systems using function splitting between distribution and remote units [6]. The proposed NGFI can be very useful to overcome drawbacks in the current fronthaul system, which is based on a digitized baseband signal transmission using interface protocols. It can be applied to 5G phase 1 networks in which RANs in sub-6-GHz bands will be deployed. However, several challenges still exist, including the extra processing latency and the capability to support advanced coordination among remote sites [7]. The lack of fiber infrastructure in dense urban and remote areas is another challenge to support ultra-dense small-cell
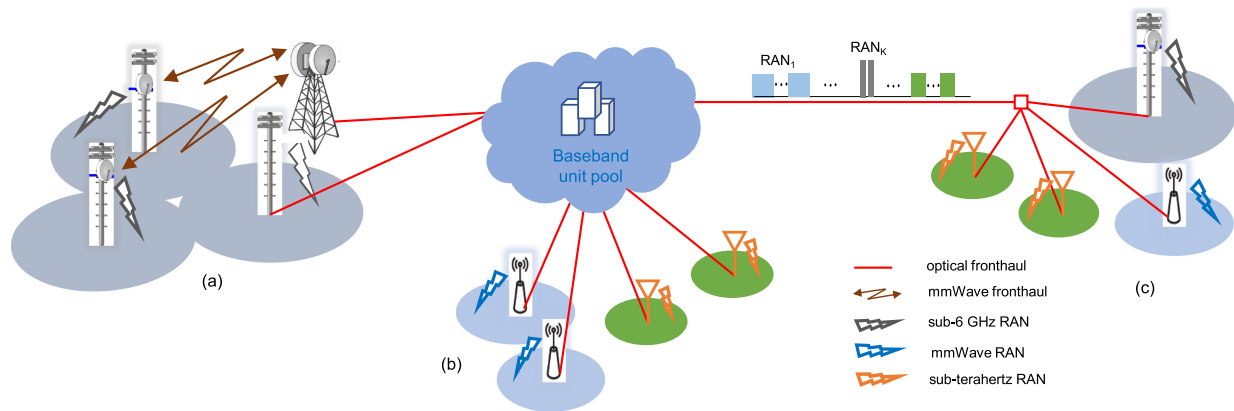
Fig. 1. Fiber–wireless converged systems for 5G and beyond networks: (a) signal encapsulation on converged fiber–mmWave system; (b) optical self-heterodyne system for mmWave RANs; (c) SCM IFoF system for multiple RAN signal transmissions.

networks. The transmission of RAN signals in high-frequency bands to a large number of antenna sites and supporting the co-existence of multiple RANs in different frequency bands will be other major challenges facing the fronthaul systems, even with the use of NGFI. Thus, a new transmission method that can exploit the cooperation between optical transport networks and RANs should be developed.

In this paper, we propose different mobile fronthaul systems for various usage scenarios by exploiting the convergence and cooperation of fiber transports and RANs. In the first system, shown in Fig. 1(a), an encapsulation of multiple RAN signals in the microwave bands on a seamlessly converged fiber and millimeter-wave (mmWave) system is presented for realizing a flexible fronthaul system where the use of fiber cables is not possible or is too expensive. This system can be useful for 4G and pre-5G networks where RANs in sub-6-GHz bands are deployed. In the second system, shown in Fig. 1(b), a converged and cooperated fiber transport and RAN system based on optical self-heterodyne (OSH) technology is proposed for the generation and transmission of RAN signals in high-frequency bands. In the third system, shown in Fig. 1(c), a subcarrier-multiplexing intermediate-frequency-over-fiber (SCM IFoF) system is proposed for the simultaneous transmission of multiple RAN signals in different frequency bands over the same optical fronthaul system.

The paper is an expanded version of the work presented in [8]. Here, new results and details of experiments are presented. For the first system, the transmission of three different services over a converged system is presented. We investigate and compare the effects of fiber dispersion on the signal transmission using single- and dual-wavelength modulation schemes. The transmission of radio signals assigned for some typical services in pre-5G networks over the systems is experimentally confirmed. In the second system, the performances of the OSH systems using different techniques at the transmitter and receiver are evaluated and compared. The effects of optical and electrical phase noises on the signal performance are also investigated. For the SCM IFoF system, the transmission of three services in the microwave, 25-GHz, and 96-GHz bands over the system is presented. The remainder of this paper is structured as follows. Section II presents and discusses the wireless signal encapsula-

tion on an mmWave link for a flexible wireless fronthaul system. In Section III, we present an OSH system and demonstrate the generation and transmission of high-speed radio signals in the 90-GHz band over the system. In Section IV, we present the SCM IFoF system and its experimental demonstrations. Finally, Section V concludes the paper.

II. SIGNAL ENCAPSULATION ON FIBER-MMWAVE SYSTEM

Wireless fronthaul systems are useful in mobile networks owing to their flexibility and ease of installation and deployment in comparison with wireline solutions. In addition, as the speed of radio waves in air is greater than that in cable media, the transmission delay can be reduced. For the realization of high-speed wireless fronthaul systems, a seamless fiber–wireless system using a radio-over-fiber (RoF) technology is a promising solution. In addition, for low-latency signal transmission, an encapsulation of analog mobile signals on the seamless fiber–wireless system can be a promising method [9]–[11]. In this section, we present the simultaneous transmission of three different radio signals, including orthogonal frequency-division multiplexing (OFDM), LTE-A, and IEEE 802.11ah signals, over the seamless system in the 90-GHz band. These three signals can represent new RAN signals for transmission of an NR below the 6-GHz band, an mMTC, and an IoT service in 5G phase 1 networks [12]. We evaluate the signal performance in terms of error vector magnitude (EVM) metric and investigate the effects of fiber dispersion in the systems using dual- and single-wavelength modulation schemes. Notably, a similar system was presented in [13], namely, a band-mapped RoF system, for the transmission of a real-time television, Wi-Fi, and baseband signal over an RoF and a 60-GHz wireless link. However, only a dual-wavelength modulation with an envelope detection at the receiver was considered. In [14], noise and nonlinear effects on the signal transmission using dual-and single-wavelength modulation were investigated. However, only one signal was transmitted over the system at a time, and the effect of fiber dispersion was not evaluated.

A. Experimental Setup

Fig. 2 presents the setup for the transmission of three wireless signals over the seamless fiber–mmWave system. First, a
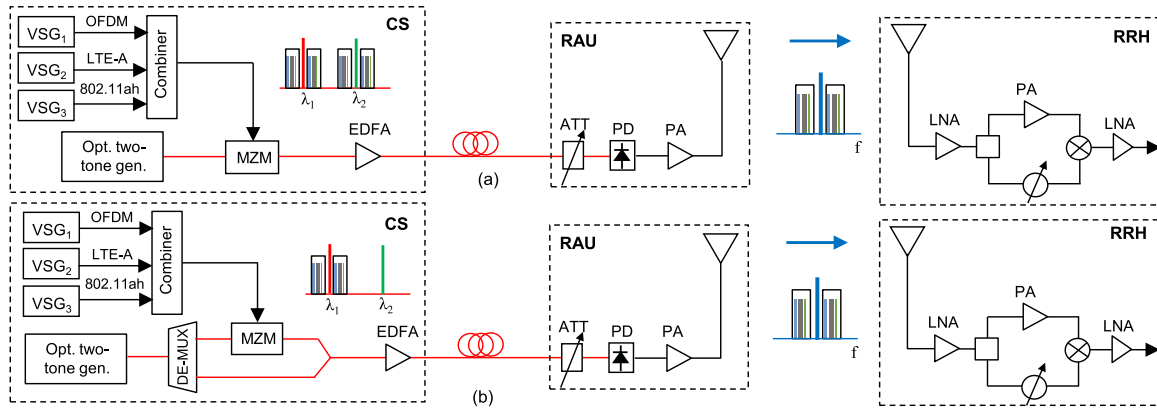
Fig. 2.   Experimental setup for signal encapsulation on a seamless fiber–mmWave system: (a) dual-wavelength modulation; (b) single-wavelength modulation.

<table>
TABLE Ia
SPECIFICATION OF TRANSMITTED RADIO SIGNALS
</table>

Signals	Carrier Freq.	Bandwidth	Modulation
OFDM	3 GHz	50 MHz	64 QAM
IEEE 802.11ah	920 MHz	10 MHz	64 QAM
LTE-A	2.6 GHz		
CC1	-	20 MHz	64 QAM
CC2	-	1.4 MHz	256 QAM
CC3	-	20 MHz	64 QAM

TABLE Ib
PARAMETERS OF THE EXPERIMENTS

Parameter	Value	Unit
Fiber length	10, 20, 30, 45	km
Optical modulation	Intensity modulation	-
mmWave distance	1	m
mmWave carrier freq.	92	GHz
Antenna gain	23	dBi
mmWave receiver	SHD	-

two-tone optical signal is generated by a high-extinction-ratio dual-parallel Mach–Zehnder interferometer modulator. Details of the signal generator are available in [15]. In this method, by setting the bias point of the main Mach–Zehnder modulator at the null point and selecting the second-order sidebands, two coherent optical sidebands with a frequency separation of quadruple the frequency of the fed synthesized electrical signal can be generated. In this experiment, an electrical synthesis signal at 23 GHz is inputted to the generator; thus, an optical mmWave signal with a frequency separation of 92 GHz is generated. For the evaluation of multiple radio signal transmissions, we generate three different radio signals with the specifications shown in Table Ia and transmit them over the system. These signals include a 50-MHz-bandwidth (BW) OFDM signal at 3 GHz, an LTE-A signal at 2.6 GHz aggregating two 20-MHz-BW carrier components (CCs) and one 1.4-MHz CC, and a 10-MHz-BW 802.11ah signal at 920 MHz. The LTE-A and the 802.11ah signals are standard-compliant, and the OFDM signal is set to emulate an NR signal having 256 subcarriers. All the signals are generated using commercially available signal studios in a computer and downloaded to vector signals generators (VSGs). The signals from the outputs of the VSGs are combined using power combiners before modulating the generated optical signals. In the dual-wavelength modulation system, both the optical sidebands of the generated two-tone optical signal are modulated by the radio signals. In the single-wavelength modulation system, only one of the optical sidebands is modulated and the other sideband remains unmodulated. In this case, the two optical sidebands are separated by an arrayed waveguide grating, and after the data modulation, the optical signals are re-combined using a 3-dB optical coupler (OC). The signals are amplified by an erbium-doped fiber amplifier

(EDFA) before being fed into a single-mode fiber (SMF) and transmitted to an optical receiver located at a remote antenna unit (RAU). At the RAU, the received optical signal is directly up-converted to a wireless signal centered at 92 GHz using a high-bandwidth photodiode (PD). The frequency fluctuation of the generated mmWave carrier signal in the system is very small and can easily follow the radio regulation [16]. After the PD, the signal is filtered using a bandpass filter and amplified using a W-band power amplifier (PA) before being emitted into free space by a 23-dBi horn antenna. After being transmitted over approximately 1 m in the air, the signal is received by another horn antenna, amplified using a low-noise amplifier (LNA), and down-converted to the original wireless signals. In our previous work [17], we confirmed that a coherent detection receiver is not suitable for the system because of high electrical phase noise. We also confirmed that an incoherent receiver using an envelope detector, such as a Schottky barrier diode (SBD), can limit the system dynamic range and the performance owing to its low receiver sensitivity and high distortion [18]. Therefore, in this experiment, we use a self-homodyne detection (SHD) receiver for the signal down-conversion. Details of the SHD are available in [18], [19]. The recovered signals are amplified using another LNA, sent to real-time spectrum analyzers (VSAs), and finally analyzed using commercially-available software [Agilent 89600 series vector signal analyzer (VSA)]. The specifications of the experimental setup are listed in Table Ib.

B. Experimental Results

We evaluate the signal performance and investigate the effects of fiber dispersion and nonlinear distortion. Fig. 3 shows the performance of the dual-wavelength modulation system.
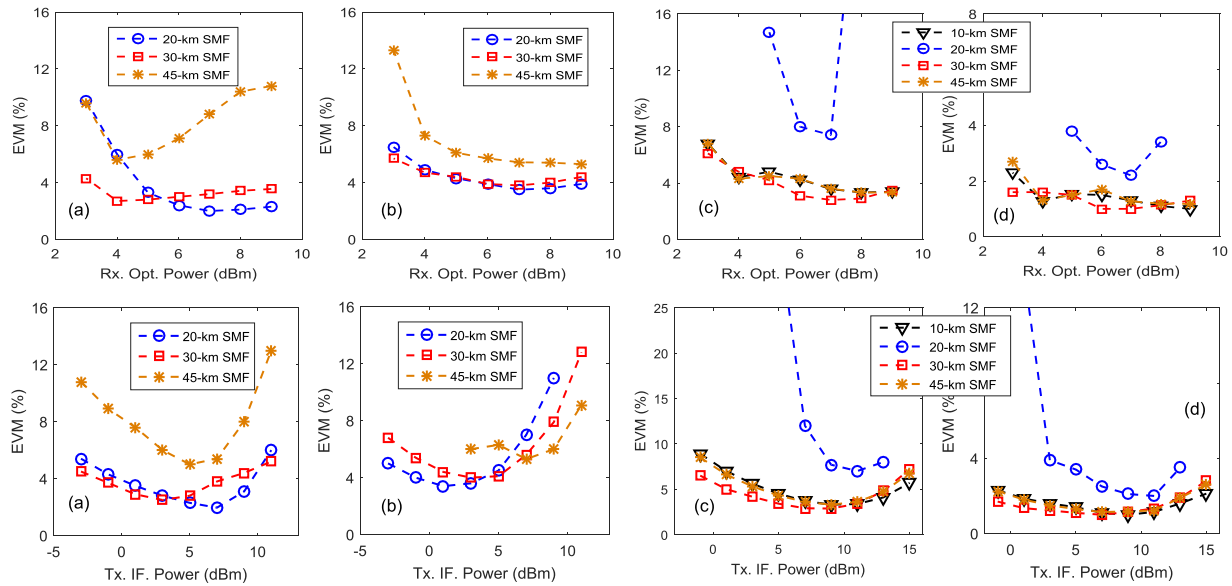
Fig. 3. Experimental results of the dual-wavelength modulation system for different received optical powers (upper) and transmit IF powers (lower): (a) 50-MHz OFDM; (b) 10-MHz 802.11ah; (c) 64-QAM 20-MHz CC LTE-A; (d) 256-QAM 1.4-MHz CC LTE-A.
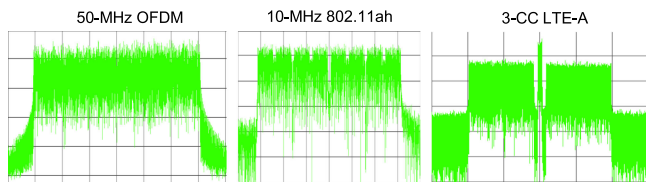

Fig. 4. Received frequency spectra of the OFDM, IEEE 802.11ah, and LTE-A signals.

Examples of the frequency spectra of the OFDM, IEEE 802.11ah, and LTE-A signals after being transmitted over the system are shown in Fig. 4. In this scheme, after the radio signals are transmitted over the system, they are re-constructed from four different beating notes of optical signals, as shown in Fig. 2(a). Thus, the bit walk-off effect induced by fiber dispersion can be large and can affect the signal performance. To investigate the effect of fiber dispersion, we transmit the signals over the seamless system using 20-, 30-, and 45-km SMFs. The upper figures show the performance for different received optical powers at the RAU, and the lower figures show the performance for different transmit powers of the radio signals. In both cases, the performance of the OFDM, 802.11ah, 20-MHz-BW LTE-A CC, and 1.4-MHz-BW CC LTE-A signals are shown in sub-figures (a), (b), (c), and (d), respectively. The performance is relatively satisfactory compared with the requirements specified in the standards. However, owing to the bit walk-off effect, the signal performance at some specific SMF lengths is significantly degraded. For instance, the performances of the OFDM signal and the 802.11ah signal are considerably degraded after the transmission over the system using a 45-km SMF, and the performance of the LTE-A signals is significantly reduced after a 20-km SMF transmission. Notably, owing to the periodical power fluctuations of fiber dispersion, both the SMF length and the carrier frequency of the radio signals contribute to the

degradation of the signal performance. For the 802.11ah signal, the performance degradation after a 45-km SMF transmission is also because the throughput drops after the long transmission [20]. From this observation, a joint optimization of fiber transmission distance and carrier frequency of the radio signals should be considered for the dual-wavelength modulation system.

We subsequently evaluate the performance of the single-wavelength modulation system, and the results are shown in Fig. 5. The upper figures show the performance for different received optical powers at the RAU, and the lower figures show the performance for different transmit powers of the radio signals. The performances of the OFDM, 802.11ah, 20-MHz CC LTE-A, and 1.4-MHz CC LTE-A signals are shown in sub-figures (a), (b), (c), and (d), respectively. Compared with the dual-wavelength modulation system, a more stable and better EVM performance can be observed. The improvement of the signal performance in this system is because of the reduction of the bit walk-off effect. As shown in Fig. 2(b), after the radio signals are transmitted over the system, they are re-constructed from only two beating notes of optical components. Therefore, for the transmission of narrow-bandwidth signals over the seamless system, a conventional optical-double-sideband modulation on a single optical sideband is appropriate to achieve satisfactory performance.

To compare the fiber dispersion effects in the dual- and single-wavelength modulation systems, we transmit and measure the power fluctuations of an IF carrier signal at different frequencies over the systems. The measurement results for the dual- and single-wavelength modulation systems are shown in Figs. 6(a) and 6(b), respectively. The powers are measured after the fiber and mmWave link transmission and are normalized to the powers of the system without inserting any SMF. In the case of the dual-wavelength modulation, several power fading dips at different carrier frequencies are observed, depending on the fiber
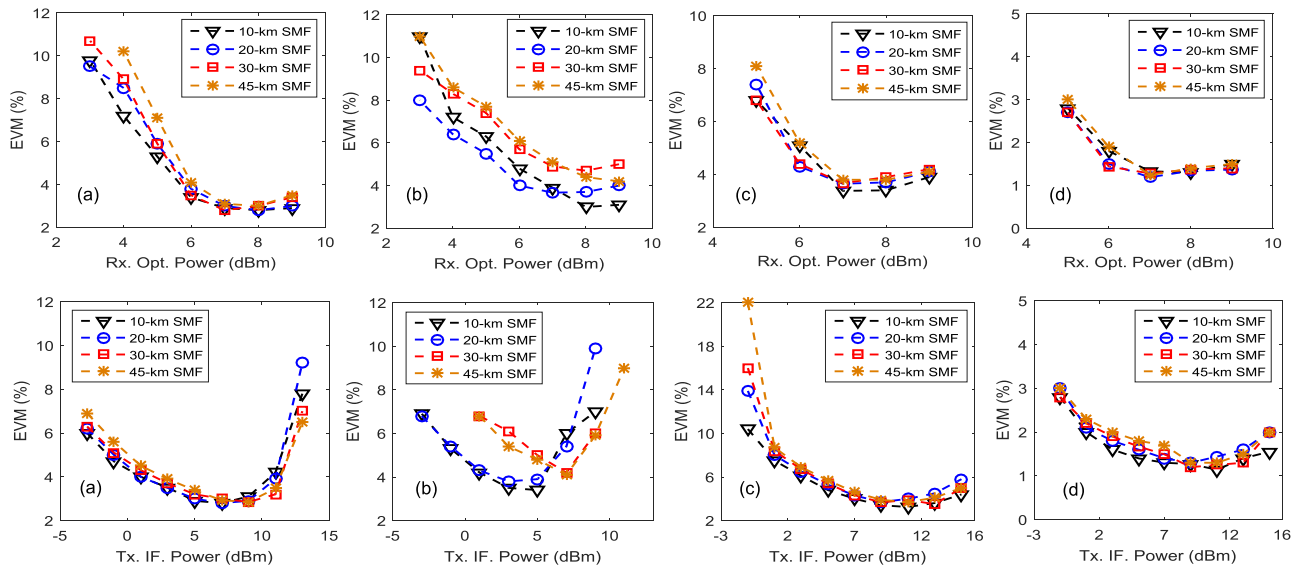
Fig. 5. Experimental results of the single-wavelength modulation system for different received optical powers (upper) and transmit IF powers (lower): (a) 50-MHz OFDM; (b) 10-MHz 802.11ah; (c) 64-QAM 20-MHz CC LTE-A; (d) 256-QAM 1.4-MHz CC LTE-A.
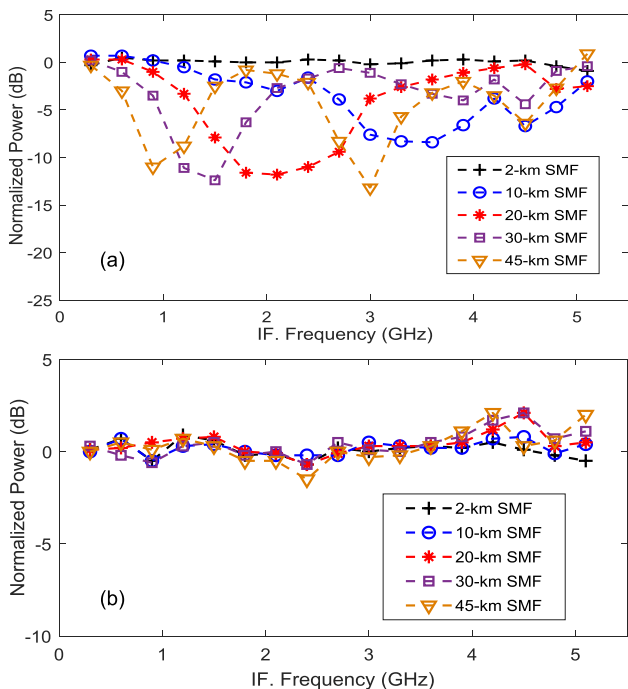

Fig. 6. Fiber dispersion effect of the system using: (a) dual-wavelength modulation; (b) single-wavelength modulation.

transmission distance. For instance, after a 20-km SMF transmission, there is a large power dip at approximately 1.5 GHz to 2.8 GHz, and after a 45-km SMF transmission, power fading dips appear at approximately 1 GHz and 3 GHz. This explains why the EVM performance of the LTE-A signal at 2.6 GHz was significantly degraded after the transmission over the 20-km SMF system, and the performances of the 802.11ah and OFDM signals were reduced after the transmission over the 45-km SMF system. In contrast, the single-wavelength modulation system does not show any significant power fading dips.

This result is consistent with the performance results shown in Fig. 5. The performance degradation of the 802.11ah signal after the transmission over the 45-km SMF system is due to the throughput reduction. Notably, in practice, the transmission distance of fronthaul systems can vary from several kilometers to tens of kilometers, depending on the latency requirement of the transmitted signals. For delay critical services, such as uRLLC, the transmission distance of fronthaul systems should be less than 20 km to satisfy an end-to-end latency requirement of less than 1 ms.

Transmission of multiple radio signals over the same fronthaul system is very important to support the co-existence of multiple RANs in the future mobile networks. In an analog waveform transport system, this can be easily implemented using the SCM technique, as shown in this experiment. In this method, radio signals at different carrier frequencies can be combined before being transmitted over the system. However, the performance of the signals can be affected by nonlinear distortions owing to a high input power. This phenomenon frequently occurs in RoF systems and can be severe in the converged fiber–mmWave systems because of the inclusion of nonlinear components, such as the optical modulator, photodetector, power amplifier, and mmWave down-converter at the receivers. Here, we evaluate the feasibility of the simultaneous transmission of three radio signals over the seamless system, and the results are shown in Fig. 7. In this measurement, we turn on the outputs of all VSGs and simultaneously transmit the three radio signals over the system. We increase the transmission powers of the other radio signals to investigate the effects of nonlinear distortion on the performance of a radio signal. The performances of the system using the dual- and single-wavelength modulation schemes are shown in the upper and lower figures, respectively. Furthermore, the performances of the OFDM, 802.11ah, 20-MHz CC LTE-A, and 1.4-MHz CC LTE-A signals are shown in sub-figures (a), (b), (c), and (d), respectively. It is observed
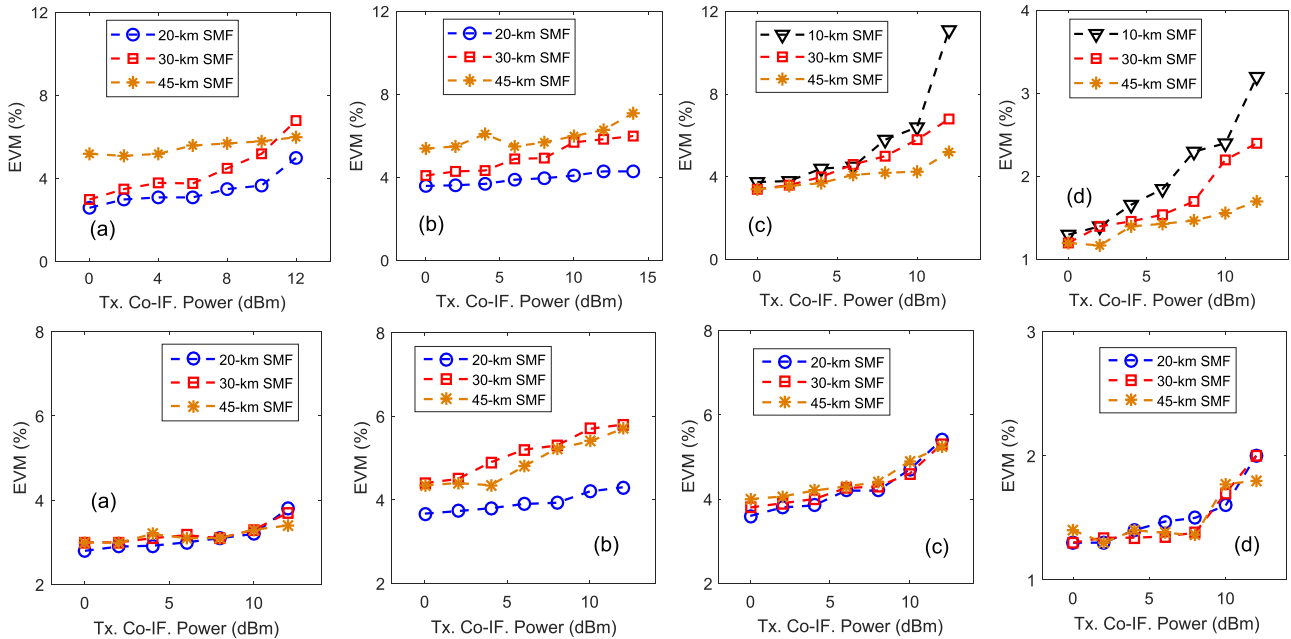
Fig. 7. Nonlinear distortion effects on the simultaneous transmission of the system using double-wavelength modulation (upper) and single-wavelength modulation (lower): (a) 50-MHz OFDM; (b) 10-MHz 802.11ah; (c) 64-QAM 20-MHz CC LTE-A; (d) 256-QAM 1.4-MHz CC LTE-A.

that increasing the transmit powers of other radio signals slightly degrades the performance of a radio signal. However, the performance degradation is not significant, and very satisfactory performance can be achieved for all signals simultaneously. In these measurements, we optimized the radio transmit power and the optical received power for each case. In this experiment, owing to the availability of signal generators, we generate and transmit three radio signals over the system. However, the encapsulation and transmission of a larger number of radio signals over the system can be achieved if the radio signals are located at appropriate IF frequencies to avoid the interference and inter-modulation distortions during the transmission.

III. OPTICAL SELF-HETERODYNE SYSTEM

As mentioned before, RANs in the mmWave bands are potential candidates for high-traffic demand and hotspot applications in 5G phase 2 and beyond networks. The transmission of mmWave RAN signals over an optical fronthaul system can be challenging owing to transmission impairments, including high fiber dispersion and nonlinear distortion effects [21]–[23]. In addition, high-speed optical modulators will be required for converting the mmWave mobile signals to optical signals, thus significantly increasing the system cost, especially when RANs in high mmWave or sub-terahertz-wave bands are used. Thus, an optical heterodyne method for the generation and transmission of mmWave radio signals over a fiber fronthaul system is a promising solution. Several works have been reported in this regard [24]–[27]. However, in these works, mmWave links worked as the transport systems; thus, powerful digital signal processing (DSP) can be employed at the receivers to compensate for the transmission impairments. In the OSH systems for the transmission of mmWave RAN signals, mmWave receivers are located at the end users; therefore, low-complexity and

simple DSP receivers are indispensable to reduce the system cost, power consumption, and latency. Thus, the development of a stable and simple OSH system with high performance is highly required.

A. Experimental Setup

The experimental setup for the generation, transmission, and up-conversion of RAN signals in the mmWave band over an optical fronthaul system is shown in Fig. 8. In this system, instead of transmitting mobile signals in the mmWave band over the fronthaul directly, the signals in a low IF band should be generated and transmitted. At the optical receiver, radio signals in high-frequency bands can be generated by up-converting the received optical signal using a high-speed PD [28], [29]. First, a two-tone optical signal is generated using high-precision optical modulation technology [15]. In this experiment, a signal with a frequency separation of 89.6 GHz between the sidebands is generated. The two optical sidebands are separated, and one of them is modulated by IF OFDM signals. The OFDM signals at 6.5 GHz, consisting of 512 subcarriers with different BWs, as shown in Table IIa, are generated in MATLAB, downloaded to an arbitrary waveform generator (AWG), and amplified using a driver amplifier before modulating the optical signal. To minimize the fiber dispersion effect, an optical IQ modulator is used to generate an optical single-sideband (SSB) signal. The modulated optical signal is amplified using an EDFA to compensate for the insertion loss and is filtered using an optical bandpass filter to reduce the amplified spontaneous emission noise. The signal is thereafter re-combined with the unmodulated optical sideband using a 3-dB OC. To avoid the effect of polarization-mode dispersion, which is incurred owing to the differential delay transmission between the modulated and unmodulated sidebands, an optical polarization controller is used to adjust
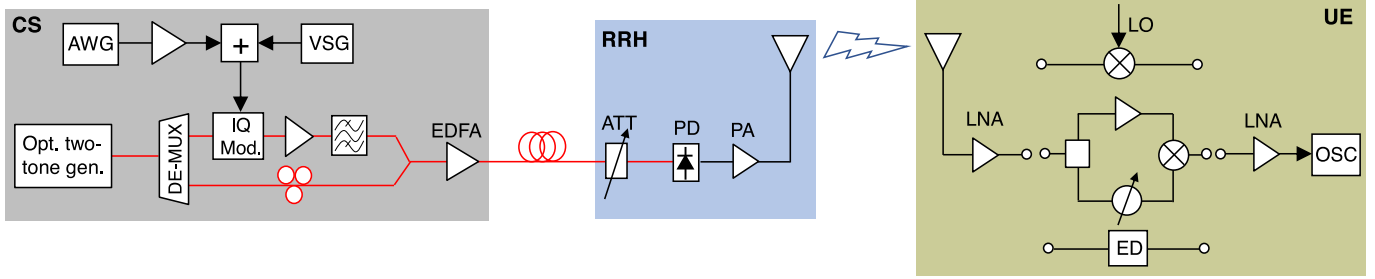
Fig. 8.   Concept of an OSH system and the experimental setup for the generation and transmission of mmWave RAN signals.

<table>
<tr><td colspan="4" align="center">TABLE IIa
SPECIFICATIONS OF SIGNALS USED IN THE OSH SYSTEM</td></tr>
</table>

Signal	IF	Bandwidth	Modulation
Single-signal transmission			
OFDM	6.5 GHz	8 GHz	16 QAM
	6.5 GHz	4 GHz	32 QAM
	6.5 GHz	2 GHz	64 QAM
	6.5 GHz	1 GHz	64 QAM
Multiple-signal transmission			
F-OFDM	2.55 GHz		
CC1, 2, 3, 4	-	800 MHz	16 QAM
LTE-A	2.6 GHz		
CC1	-	20 MHz	64 QAM
CC2	-	20 MHz	256 QAM

<table>
<tr><td colspan="3" align="center">TABLE IIb
SPECIFICATIONS OF THE OSH SYSTEM EXPERIMENTS</td></tr>
</table>

Parameter	Value	Unit
Single-signal transmission		
Fiber length	10, 20, 30	km
Optical modulation	Optical SSB	-
mmWave distance	1	m
mmWave carrier freq.	96.1	GHz
mmWave receiver	Coherent, SHD, SBD	-
Multiple-signal transmission		
Fiber length	20	km
Optical modulation	Intensity modulation	-
mmWave distance	1	m
mmWave carrier freq.	90.8	GHz
mmWave receiver	Coherent	-

the polarization state of the unmodulated signal. The combined optical signal is amplified using another EDFA before being transmitted over an SMF to an optical receiver, which is located at a remote radio head (RRH). At the RRH, an optical variable attenuator is used to adjust the received optical power before the signal is inputted to a high-speed PD for up-converting to mmWave radio signals. The signal is filtered using a bandpass filter and amplified using a PA before being transmitted into the air by a horn antenna. After being transmitted over approximately 1 m in free space, the signal is received by another horn antenna, which is located at the user equipment (UE) in practical systems and amplified using an LNA before being down-converted. For the signal down-conversion, a coherent detection using an electrical mixer is used to increase the receiver sensitivity for the wideband signal detection. To reduce the optical and electrical phase noises, incoherent detections using an SBD and an SHD are also used. After being down-converted, the signal is amplified using an LNA, sent to a real-time oscilloscope (OSC), and is finally demodulated in MATLAB. The parameters of the experimental setups are summarized in Table IIb.

B. Experimental Results

In the OSH systems, optical sidebands at the output of the two-tone optical signal generator are phase-correlated. However, after the fiber transmission, owing to fiber dispersion effects, the two optical signals experience a differential propagation delay, which can be calculated as [30]

$$\Delta\tau_{disp} = D.L.\frac{\lambda^2}{c}.f_{mmWave}, \tag{1}$$

where D is fiber dispersion, L is the fiber transmission distance, λ is the wavelength, c is the speed of light in vacuum, and f_{mmWave} is the frequency of the mmWave carrier signal. In addition, for the data modulation, the two optical signals are separated and propagated via separate optical paths before being combined into the same fiber; therefore, they experience an additional differential propagation delay, which is calculated as [30]

$$\Delta\tau_{path} = \pm\frac{\Delta L_{path}}{c}.n, \tag{2}$$

where ΔL_{path} is the path length difference and n is the refractive index of the device material.

The two differential delays are combined, resulting in a state of partial phase decorrelation, which leads to an increase in the phase noise and the carrier-to-noise ratio (CNR) penalty of the generated mmWave carrier signals. The CNR penalty induced by the differential delays is calculated as [30]

$$\Delta_{CNR} = 10\log\left(\frac{1}{\exp^{-2\pi.\Delta\tau_{tot}.\Delta\vartheta_m}}\right), \tag{3}$$

where $\Delta\tau_{tot}$ is the sum differential delay of (1) and (2), and $\Delta\vartheta_m$ is the full-width half-maximum linewidth of the laser used for the two-tone optical signal generation. The phase noise induced by the differential delay is expressed as the rms phase
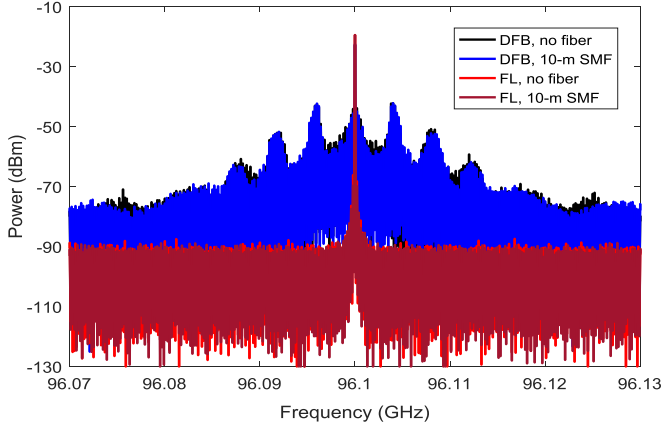
Fig. 9.   Spectra of the generated mmWave carrier signals at 96.1 GHz.

error and is given by [30]

$$(\sigma_{\emptyset})^2_{delay} = \int_0^{B_n} \frac{2\Delta\vartheta_m}{\pi.f^2} \left[1 - cos\left(2\pi.f.\Delta\tau_{tot}\right) \right] df$$

$$\approx 2.\pi.\,\Delta\vartheta_m.B_n.\left(\Delta\tau_{tot}\right)^2, \tag{4}$$

where B_n is the noise bandwidth of the mmWave receivers.

Using (3), we can estimate the CNR penalty in different cases. For example, for the transmission over a 30-km SMF link with an optical path difference of 10 m, the mmWave signal at 96.1 GHz has a CNR penalty of approximately 14 dB and 0.00002 dB using a laser having a linewidth of 10 MHz and 15 Hz, respectively. Notably, in this case, the optical path imbalance delay is dominant. The increase in the phase noise results in the broadening of the generated mmWave carrier signal after the optical beating at the PD and can significantly reduce the signal performance. The spectra of the generated 96.1-GHz carrier signal at the output of the PD for the system using a 10-MHz-linewidth distributed feedback (DFB) laser and a 15-Hz-linewidth fiber laser (FL) are shown in Fig. 9. In the measurement, only the carrier signal of the IF signal is transmitted. In the figures, we compare the results when no fiber or a 10-m-SMF cable is inserted to the unmodulated optical sideband to compensate for the optical path imbalance. For the system using the FL, owing to its narrow linewidth, a very narrow linewidth mmWave carrier signal can be generated. However, in the system using the DFB, the large phase noise of the laser interplays with the differential delay, resulting in the partial phase decorrelation and broadening of the generated mmWave carrier signal. We measure the SSB phase noise characteristics of the generated mmWave carrier signal. Figs. 10(a) and 10(b) show the results for the system using the FL after an optical back-to-back and a fiber transmission (a 30-km SMF is inserted into the system as an example of the fiber transmission), respectively. The results for the system using the DFB laser are shown in Figs. 10(c) and 10(d), respectively. In each figure, we compare the results when no fiber cable, a 5-m fiber cable, and a 10-m fiber cable are inserted to the unmodulated optical sideband to compensate for the differential transmission delay. It is observed that the phase noise of the system using the FL is very stable and the results

are relatively constant in all cases. At a frequency offset of 1 MHz, a low phase noise of approximately −110 dBc/Hz can be achieved. In contrast, the phase noise of the system using the DFB is relatively high, and the result for the case of inserting a 10-m fiber to the unmodulated sideband is slightly better. At a frequency offset of 1 MHz, a large phase noise of approximately −75 dBc/Hz is observed. To compensate for the phase noise in the system using a coherent detection, strong phase noise compensation algorithms should be employed [31], [32]. However, this inclusion significantly increases the complexity, power consumption, and latency of the receivers. Other phase noise compensation technologies, such as that in [33], can be applied; however, the implementation is not easy and not practical for mobile fronthaul systems.

We thereafter investigate the signal performance after it is transmitted over the optical fronthaul and the radio access link. Fig. 11 shows the performance of the OFDM signals. In this measurement, the 15-Hz FL is used for the two-tone optical signal generation, and the coherent detection by an electrical mixer is used at the receiver. To evaluate the system performance for the transmission of different wideband signals, including signals having different BWs and modulation orders, we generate OFDM signals with a 1-GHz, 2-GHz, 4-GHz, and 8-GHz BW as the examples and transmit them over the system. Owing to the high performance of the system, for 1- and 2-GHz-BW signals, 64-QAM modulation can be applied. For the 4-GHz-BW signal, the EVM performance can satisfy the requirement for 32-QAM modulation. For the 8-GHz-BW signal, 16-QAM signal can be generated and transmitted successfully over the system. Owing to the use of the SSB optical modulation in a single-wavelength modulation, the effect of fiber dispersion is negligible and the performances of the transmission over the system using 10-, 20-, and 30-km SMF are relatively similar. The results show that the OSH method is a promising method for the transmission of mmWave RAN signals over the optical fronthaul with low fiber dispersion effects and satisfactory performance. Notably, the specifications of the transmitted signals and the parameters of the experimental setup used in this experiment are designed to show the capability of the system in different cases and have not yet been fully optimized. With this method, it is possible to provide an adaptive generation and transmission of mobile signals using appropriate bandwidths and modulation levels, depending on the transmission conditions and demands.

However, the results shown in Fig. 11 are achieved only when a very narrow-linewidth laser is used. When the DFB laser with a linewidth of approximately 10 MHz is used, it is not possible to demodulate the signals owing to the broadened linewidth and the increased phase noise of the carrier signal, as shown in Figs. 9 and 10. The use of narrow-linewidth lasers is a simple method to achieve high performance. However, the cost of the system can be significantly increased owing to the high cost of the lasers. The use of inexpensive lasers should be considered to reduce the system cost. To reduce the phase noise effects, an incoherent detection at the receiver can be used. However, the receiver sensitivity and the system dynamic range of this method are limited; thus, the signal performance and the transmission range of the radio links can be significantly reduced.
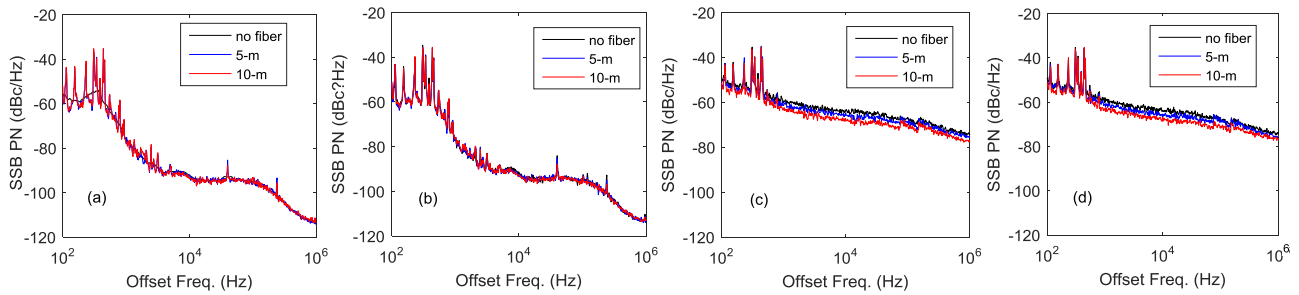
Fig. 10.   Single-sideband phase noise of the generated carrier signal at 96.1 GHz: (a) using FL with an optical back-to-back; (b) FL with a 30-km SMF; (c) DFB laser with an optical back-to-back; (d) DFB laser with a 30-km SMF.
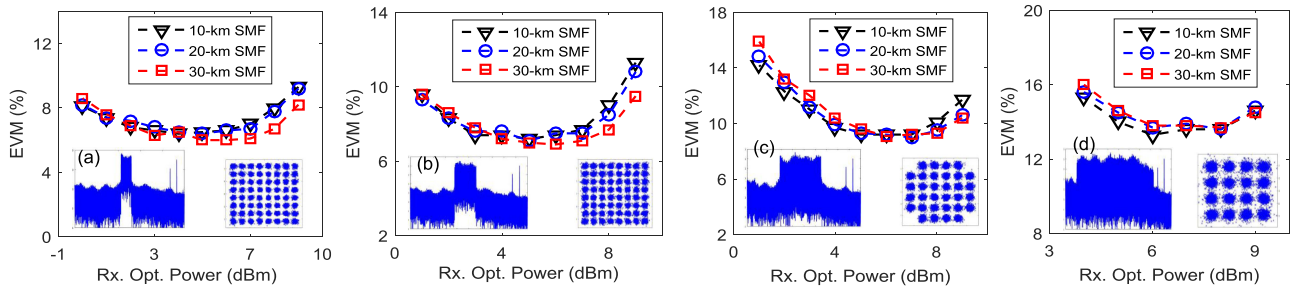

Fig. 11.   Performance of OFDM signals after being generated and transmitted over the system using a 15-Hz FL: (a) 64-QAM 1-GHz-BW signal; (b) 64-QAM 2-GHz-BW signal; (c) 32-QAM 4-GHz-BW signal; (d) 16-QAM 8-GHz-BW signal.
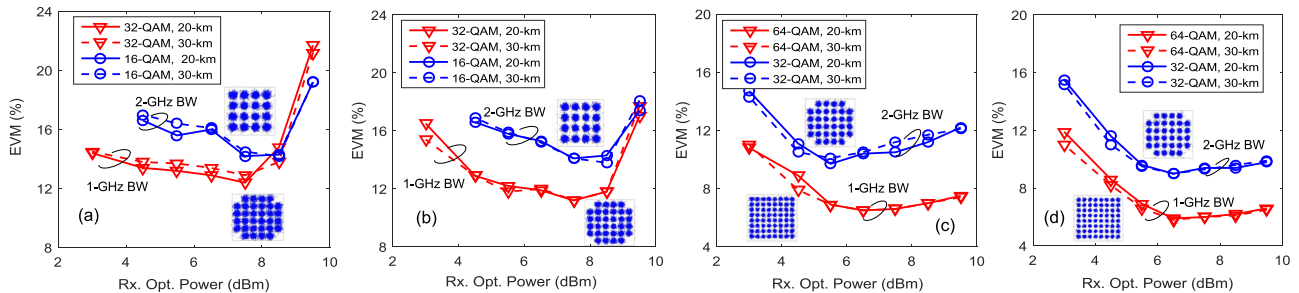

Fig. 12.   Signal performance after the transmission over the system using: (a) SBD and DFB; (b) SBD and FL; (c) SHD and DFB; (d) SHD and FL.

Thus, an SHD detector can be a promising alternative. Fig. 12 compares the performance of the system using the SBD and the SHD as the signal down-converter at the receiver. Owing to the bandwidth limitation of the SHD, we limit the signal bandwidth to 1 and 2 GHz. The SBD is a zero-bias Schottky diode with a full bandwidth in the W band. The performance of the system using the SBD at the receiver and the DFB and the FL at the transmitter is shown in Figs. 12(a) and 12(b), respectively, and those of the system using the SHD at the receiver and the DFB and the FL at the transmitter is shown in Figs. 12(c) and 12(d), respectively. It is observed that, using the incoherent and self-homodyne methods, the phase noise induced by the differential transmission delay and the laser phase noise can be cancelled out, and the performances of the system using the DFB and the FL are relatively similar. In addition, owing to the better receiver sensitivity and dynamic range, the SHD system demonstrates a much better performance, and high-modulation signals can be transmitted and received. The results show that mmWave mobile signals can be generated and transmitted with satisfactory

performance using the OSH system with the SHD at the receiver. The system is relatively simple and inexpensive; thus, it can be appropriate for mobile fronthaul transmission. Notably, the OFDM signals used in this experiment do not include any strong phase noise and fiber dispersion compensations, which is suitable for RAN signals in the future mobile networks. In these systems, fiber dispersion and phase noise effects should be optimized in the systems instead of being optimized by the DSP at the receivers. This is different from the current systems where the receivers are located at RRHs, and a strong DSP can be employed to compensate for the transmission impairments.

Furthermore, the generation and transmission of multiband radio signals by the optical heterodyne systems can be realized. In addition, the transmission of multiple RAN signals over the same mobile fronthaul is important to reduce the number of fiber links. We investigate the generation and transmission of multiband and multiple RAN signals over the same optical fronthaul using the OSH system. In the experiment, a four-CC signal, as an example of multiband signal generation and transmission
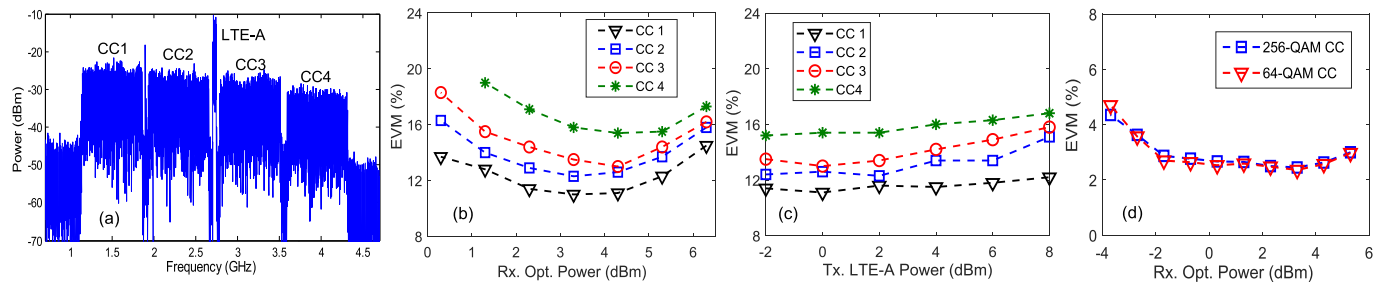
Fig. 13. Performance of multiband OFDM and LTE-A signals after the transmission over the system: (a) received frequency spectrum; (b) multiband OFDM versus received optical powers; (c) multiband OFDM signal versus transmit power of LTE-A signal; (d) LTE-A signal versus received optical power.

over the system, is generated in MATLAB and downloaded to an AWG. The CCs are placed next to each other using a filtered OFDM (F-OFDM) method [34]. An empty gap of 50 MHz is inserted between the second and third CCs to insert an LTE-A signal, which consists of two 20-MHz CCs, and is generated by a VSG. The specifications of the transmitted signals are listed in Table IIa. The OFDM and LTE-A signals are combined using a power combiner and they modulate an optical sideband, as shown in Fig. 8. In this experiment, an optical intensity modulator is used for the optical signal modulation instead of using an optical IQ modulator [34]. The parameters of the experimental setup are listed in Table IIb. Examples of the signal performance are shown in Fig. 13 for the OFDM and LTE-A signals. Fig. 13(a) shows the frequency spectrum of the received signal, consisting of the four-band OFDM and LTE-A signals. Figs. 13(b) and 13(c) show the performance of the OFDM signals for different received optical powers and different transmit powers of the LTE-A signal, respectively. Satisfactory performance could be confirmed for 16-QAM OFDM signals carried by all the CCs. The performance of the signals at high frequencies is relatively degraded because of the non-flat frequency response of the system. Increasing the transmitting power of the LTE-A signal has a small impact on the performance of the OFDM signals. The performance of the LTE-A signals is shown in Fig. 13(d) for different received optical powers. All the signals are successfully transmitted with EVM values much better than the requirements specified in the standard, i.e., 8% for 64-QAM and 3.5% for 256-QAM signals. In this measurement, the LTE-A signal is measured after the optical fronthaul and the mmWave access link; however, we can easily extract and evaluate it only after the optical fronthaul system.

IV. SUBCARRIER MULTIPLEXING IFoF SYSTEM

The co-existence of multiple RANs at different frequency bands is very important in 5G and beyond networks [35]. LTE-A with new releases and NRs below the 6-GHz bands can provide high data rate and large coverage communications in pre-5G networks. New RANs using new waveforms and multiple access methods in low-mmWave bands, such as up to 30-GHz bands, can be deployed to provide high data rate, massive connectivity, and low latency use cases in 5G phase 1 networks by the year 2020. In addition, RANs in high-mmWave bands and sub-terahertz-wave bands can be deployed for hotspot and massive traffic areas in beyond 5G networks after the year 2020. To re-
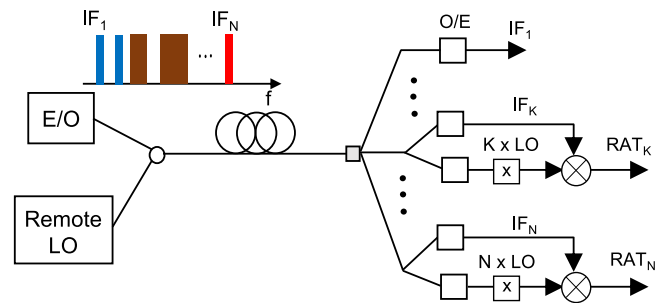

Fig. 14. Concept of an SCM IFoF system and its application for multiple RAN signal transmissions.

alize such application scenarios, an efficient fiber transmission system from a cloud to many remote sites is of paramount importance. A digitized baseband signal transmission requires very high data rate fiber links and complicated remote sites. RoF systems require expensive high-bandwidth optical components and are vulnerable to the fiber dispersion and distortion effects. In the previous section, we presented the generation and transmission of RAN signals in the mmWave and microwave bands using the OSH system. However, the transmission is limited to a RAN signal in the mmWave band and the other RAN in the microwave band. For the transmission of multiple RAN signals in different high-frequency bands, the system is not scalable. A simple, low-cost, and high-spectral-efficiency system using an SCM IFoF system with a remote delivery of local oscillator (LO) signals can be a promising solution [36]. In this system, as shown in Fig. 14, different signals can be mapped to different IFs in the electrical domain before modulating a lightwave signal. An appropriate LO signal can also be delivered remotely from the central station for up-converting the signals to appropriate frequency bands at antenna sites. At the antenna sites, IF signals can be mixed with the LO signals to generate the RAN signals in the desired frequency bands. These LO signals can be generated flexibly from the originally transmitted LO signal using electrical frequency converters. This method can provide a cost-effective and scalable solution for the simultaneous transmission of multiple radio signals in the future mobile networks.

Notably, a wavelength-division-multiplexing IFoF system can provide a simple system in which each radio signal can be fed to a wavelength for being transmitted to appropriate antenna sites. However, with the deployment of ultra-dense small cells and the need to transport a large traffic volume for massive MIMO and carrier aggregation in the future mobile
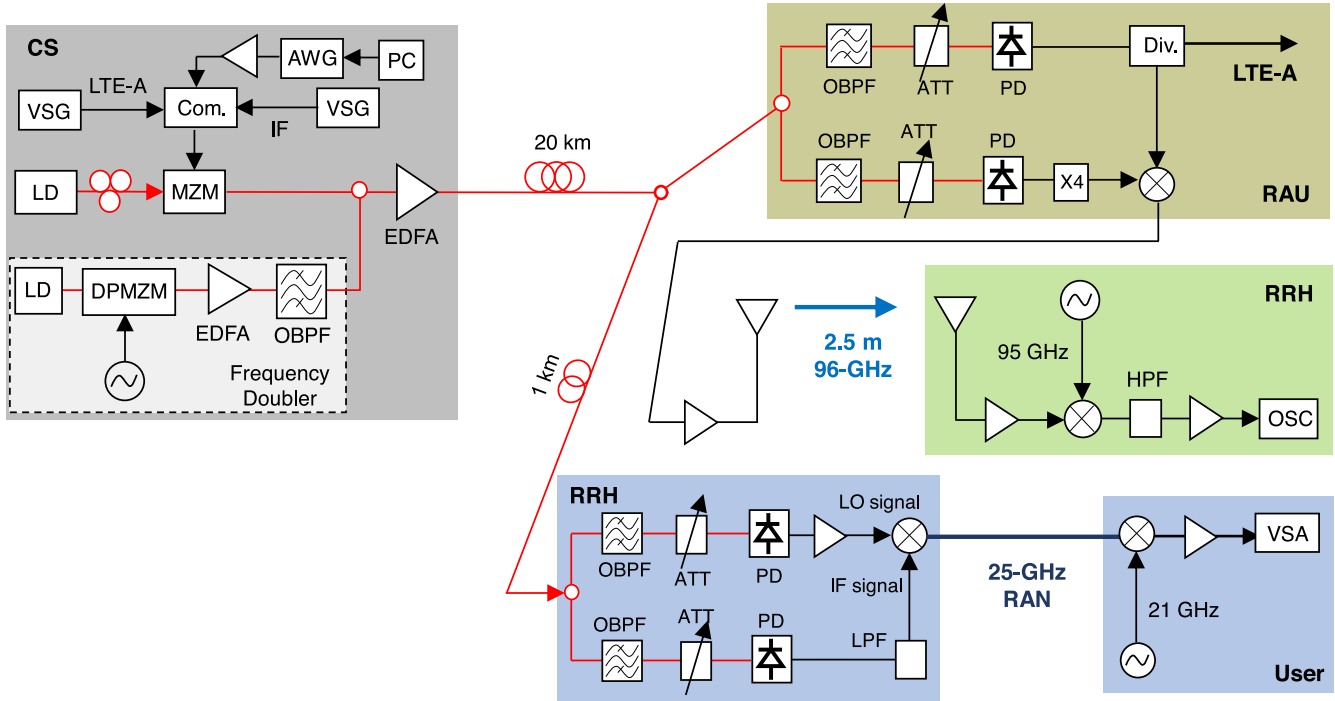
Fig. 15.   Experimental setup for the simultaneous transmission of an LTE-A, a 25-GHz, and a 96-GHz radio signal over the SCM IFoF system.

TABLE III
PARAMETERS OF SIGNALS IN THE SCM IFoF SYSTEM

Signal	IF	Bandwidth	Modulation
OFDM	2 GHz		
CC1	-	400 MHz	16 QAM
CC2	-	400 MHz	16 QAM
CC3	-	400 MHz	16 QAM
CC4	-	400 MHz	16 QAM
LTE-A	1.94 GHz		
CC1	-	20 MHz	256 QAM
CC2	-	20 MHz	256 QAM
CC3	-	10 MHz	256 QAM
OFDM/FBMC	1 GHz	50 MHz	64-QAM

Fig. 16.   (a) Spectrum of optical signal; (b) frequency spectrum of received signal (before being filtered).

networks, optical resources can be exhausted. Especially, in the areas where the optical wavelengths are fully used, the reuse of the deployed optical resources is very important for easy and quick deployment of new RANs. In [37], a transmission of base-band, microwave band, and 60-GHz band over a fiber link was implemented using an RoF system. However, it was relatively difficult to optimize the performance for all signals, and the system was not scalable to the frequency of the mmWave signals. An all-band RoF system was also proposed for the multiple-service transmission over a fiber link [13], [38]; however, the optical spectral efficiency is low [38], and proper PDs and am-plifiers must be used to filter out unwanted beating signals [13]. It was also relatively difficult and not scalable for the transmis-sion of multiple mmWave signals in different frequency bands. Thus, the SCM IFoF system with an electrical up-conversion is a very promising solution. In [39], an IFoF system with a remote LO signal transmission was reported for a 28-GHz RAN signal
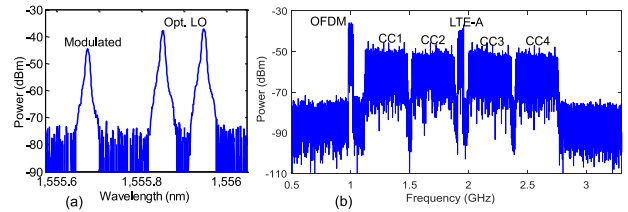
transmission. However, the LO signal was transmitted together with the IF signals at the same wavelength, and the system is not scalable for multiple RAN signal transmissions.

A. Experimental Setup

The experimental setup for the simultaneous transmission of three different radio signals, including an LTE-A signal at 1.94 GHz, an OFDM signal at 25 GHz, and an F-OFDM signal at 96 GHz over an SCM IFoF system is shown in Fig. 15 [36]. The specifications of the transmitted signals in this experiment are listed in Table III. The radio signals in these frequency bands are used to emulate the transmission of RAN signals in differ-ent frequency bands, including those in the microwave band, low-mmWave bands, and high-mmWave bands, which can be deployed in pre-5G, 5G, and beyond 5G networks, respectively. The LTE-A signal aggregating three CCs at 1.94 GHz and the OFDM signal with a BW of 50 MHz at 1 GHz are generated by VSGs. The F-OFDM signal aggregating four 400-MHz-BW CCs is generated in MATLAB and downloaded to an AWG. The F-OFDM signal can represent the mapping of different
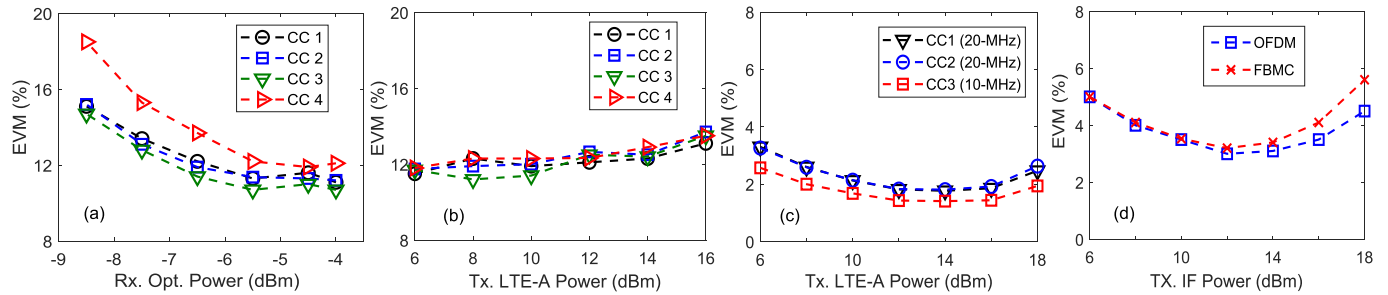
Fig. 17. Signal performance after transmission over the system: (a) 96-RAT F-OFDM signal vs. received optical powers; (b) 96-RAT F-OFDM signal vs. LTE-A transmit powers; (c) LTE-A signal at 1.94 GHz; (d) 25-GHz RAT signal.

CCs or different MIMO signal components and can be flexibly arranged so that the LTE-A and OFDM signals can be inserted at appropriate positions. The generated signals are combined using power combiners before modulating a lightwave signal from a laser diode at an optical modulator. In this experiment, for simplicity, we use an optical intensity modulator for converting radio signals to optical signals. However, an IQ optical modulator, which is similar to the one shown in Fig. 8, can be used to generate an optical SSB signal to reduce the fiber dispersion effects. In addition, an optical LO signal is generated by a frequency doubler using a dual-parallel Mach–Zehnder interferometer modulator. In contrast to the signal generator shown in Fig. 8, the main MZM is biased at the full point so that the first-order sidebands can be generated. The modulated signal and the optical LO signal are combined using a 3-dB OC, amplified using an EDFA, and transmitted to a division point via a 20-km SMF. At the division point, the optical signals are divided (using an optical splitter in this experiment) to transmit the optical signals to different RRHs. In this experiment, we consider that the LTE-A and 96-GHz RAN signals are detected from the same optical signal. However, we can further divide the optical signal to transmit to different RRHs. At the RRH for the LTE-A and 96-GHz signals, the optical signals are separated to recover the LO and the modulated optical signals using optical bandpass filters. After being converted to electrical formats using PDs, the LTE-A signal can be detected and sent to a VSA for signal demodulation and analysis. The detected F-OFDM signal is up-converted to a radio signal at 96 GHz band by being mixed with the 96-GHz LO signal. This 96-GHz LO signal is generated by inputting the 24-GHz signal, which is generated from the optical LO signal, to a frequency quadrupler. The up-converted signal is amplified using a PA before being emitted into free space by a 23-dBi horn antenna. After transmission over approximately 2 m in free space, the signal is received by another antenna, amplified, and down-converted using a coherent detection. The down-converted signal is filtered using a high-bandpass filter to avoid the DC component, amplified, and sent to a real-time OSC. Finally, the signal is demodulated in MATLAB. At the RRH for the 25-GHz RAN, the received optical signal is divided using a 3-dB OC to recover the LO and the IF signals. After being converted to electrical formats, a RAN signal at 25 GHz is generated by mixing the signals together using an electrical balanced mixer. In practical systems, this RAN signal can be fed to an antenna and transmitted to end users.

However, in our experiment, owing to the lack of antennas in the 25-GHz band, we transmit the signal over an RF cable, and down-convert to an IF band. Finally, the signal is sent to a VSA and demodulated using the VSA software.

B. Experimental Results

The optical spectra of the signal transmission are shown in Fig. 16(a), consisting of the optical LO signal with a frequency separation of 24 GHz between the sidebands and the modulated optical signal. Fig. 16(b) shows the frequency spectra of the received electrical signal, measured at the receiver for the LTE-A signal. Figs. 17(a) and 17(b) show the performance of the F-OFDM signals for different received optical powers and transmit powers of the co-transmission LTE-A signal, respectively. In this experiment, a four-band F-OFDM signal with a BW of 400 MHz for each sub-band is generated and transmitted over the system as an example of multiband signal generation and transmission. The signals carried by the CCs can be independent. However, for the sake of simplicity, in the experiment, we generate the four signals with the same parameters, including 256 subcarriers of which 8 subcarriers are for pilots and 17 subcarriers at each band edge are null. Satisfactory performance could be confirmed for 16-QAM signals. The performance of the signal in CC4 is relatively degraded, especially when the received optical power is reduced, owing to the non-flat frequency response of the system. Increasing the transmit power of the LTE-A signal has a relatively small impact on the performance of the F-OFDM signals. Fig. 17(c) shows the EVM performance of 256-QAM LTE-A signals carried by different CCs. The transmission can easily satisfy the requirement with a sufficiently large power range. Fig. 17(d) shows the performance of the 25-GHz signal after transmission over the fiber system at different transmit powers. The figure shows the performance of both OFDM and filter bank multicarrier (FBMC) signals. The measured EVM values are well below the requirement for a 64-QAM signal. The effect of fiber dispersion on the signal transmission is relatively small owing to the transmission of signals in low IF bands over the fiber link.

The satisfactory performance of all signals after being combined and transmitted over the optical fronthaul system using the SCM IFoF and the electrical up-conversion at antenna sites present an effective method for the co-existence of multiple RANs in the future mobile networks, especially in 5G phase 2

and beyond networks. The system can be further optimized to improve the signal performance and to transmit high-speed RAN signals, such as using advanced optical modulation techniques and a better LO signal generation. In this experiment, the LO signal for up-converting the signal to 96-GHz band has a relatively high noise floor, which is generated by the frequency quadrupler. In a practical system, by using a well-tailored narrow-band frequency converter that can be designed appropriately for the LO signal generation, the noise level of the generated LO signal at antenna sites can be significantly reduced; thus, the performance of the high-frequency RAN signals can be improved. The system is cost-effective because optical components at low speed can be used for the transmission and generation of high-frequency radio signals. In addition, low fiber dispersion effects and high-spectral-efficiency systems can be realized by transmitting signals in the low-frequency bands over the optical fronthaul links. Notably, the RANs in this experiment, including those at 1.94 GHz, 25 GHz, and 96 GHz, are chosen to investigate the capability of the system for the transmission of different RANs at different frequency bands. The system can support a flexible co-existence and transmission of RAN signals in different frequency bands through a joint optimization of the LO signal generation and the IF signal mapping on the optical channel. For the LO signal generation, the frequency of the LO signal can be flexibly varied by changing the frequency of the input electrical signal at the transmitter. For the subcarrier multiplexing of IF signals, owing to the flexibility of the F-OFDM signal generation, the IF signals can be mapped to appropriate bands to be transmitted to the antenna sites. The optimal arrangement plans of IF signals on a fiber link were investigated in [40]. At the antenna sites, the IF signals can be up-converted to the desirable RANs by mixed them with the generated LO signals.

V. CONCLUSION

We have presented different mobile fronthaul systems for the future mobile networks using seamless convergence fiber-optic and wireless systems. In the first solution, a flexible wireless fronthaul system can be realized using an encapsulation of wireless signals in the microwave bands onto a converged fiber–mmWave system. We successfully transmit and demodulate three different wireless signals over the system and investigate the effects of fiber dispersion and nonlinear distortion on the signal performance. The proposed system can be useful for the transmission of radio access signals in dense small-cell networks where the use of a fiber cable is not feasible. In the second solution, we present and investigate the performance of an OSH system for the generation and transmission of radio access signals in high-frequency bands. We discuss the effects of optical and electrical phase noises, and compare the performance for different cases, including the use of different laser types at the transmitter and detection methods at the receiver. A high-performance system can be realized using a narrow-linewidth laser at the transmitter, and/or a self-homodyne detection at the receiver. The system can be a promising solution for the transmission of RAN signals in high-frequency bands,

such as at 100 GHz over more, in 5G beyond networks. Finally, an efficient fronthaul system for the simultaneous transmission of multiple RAN signals in different frequency bands using a subcarrier multiplexing IFoF system is proposed. By generating and mapping different RAN signals onto appropriate IFs, multiple radio signals can be transmitted over a fiber fronthaul system simultaneously. Satisfactory performance of the proposed systems reveals the potential of the seamless convergence and cooperation between fiber transport and radio access networks.

REFERENCES

[1] 3GPP TR 38.913 V14.2.0: "Study on Scenarios and Requirements for Next Generation Access Technologies," Mar. 2017.

[2] Draft new report ITU-R M. [IMT-2020.SUBMISSION]: "Requirements, evaluation criteria and submission templates for the development of IMT-2020," Jun. 2017.

[3] [Online]. Available: http://www.5gtf.net/

[4] J. Lee et al., "Spectrum for 5G: Global status, challenges, and enabling technologies," IEEE Commun. Mag., vol. 56, no. 3, pp. 12–18, Mar. 2018.

[5] I. F. Akyidiz et al., "Combating the distance problem in the millimeter wave and terahertz frequency bands," IEEE Commun. Mag., vol. 56, no. 3, pp. 102–108, Mar. 2018.

[6] C.-L. I et al., "RAN revolution with NGFI (xhaul) for 5G," J. Lightw. Technol., vol. 36, no. 2, pp. 541–550, Jan. 2018.

[7] K. Miyamoto et al., "Split-phy processing architecture to realize base station coordination and transmission bandwidth reduction in mobile fronthaul," presented at the Opt. Fiber Commun. Conf. Exhib., Los Angeles, CA, USA, 2015, Paper M2J.4.

[8] P. T. Dat et al., "Radio-over-fiber-based seamless fiber-wireless convergence for small cell and linear cell networks," presented at the Opt. Fiber Commun. Conf. Expo., San Diego, CA, USA, 2018, Paper M4J.5.

[9] A. Kanno et al., "Radio-on-terahertz over fiber system for future mobile fronthauling," in Proc. IEEE Global Telecommun. Conf., 2014, pp. 2218–2222.

[10] M. Xu et al., "Bidirectional fiber-wireless access technology for 5G mobile spectral aggregation and cell densification," J. Opt. Commun. Netw., vol. 8, no. 12, pp. B104–B110, 2016.

[11] P. T. Dat et al., "Radio-on-radio-over-fiber: Efficient fronthauling for small cells and moving cells," IEEE Wireless Commun., vol. 22, no. 5, pp. 67–75, Oct. 2015.

[12] A. Ghosh, "5G new radio (NR): Physical layer overview and performance," in Proc. IEEE Commun. Theory Workshop, May 2018.

[13] M. Zhu et al., "Radio-over-fiber access architecture for integrated broadband wireless services," J. Lightw. Technol., vol. 31, no. 23, pp. 3614–3620, Dec. 2013.

[14] J. James et al., "Nonlinearity and noise effects in multi-level signal millimeter-wave over fiber transmission using single and dual wavelength modulation," IEEE Trans. Microw. Theory Techn., vol. 58, no. 11, pp. 3189–3198, Nov. 2010.

[15] T. Kawanishi et al., "High-speed control of lightwave amplitude, phase, and frequency by use of electrooptic effect," IEEE J. Sel. Topics Quantum Electron., vol. 13, no. 1, pp. 79–91, Jan./Feb. 2007.

[16] A. Kanno et al., "Evaluation of frequency fluctuation in fiber-wireless link with direct iq down-converter," presented at the Eur. Conf. Opt. Commun., 2014, Cannes, France, Paper We.3.6.3.

[17] P. T. Dat et al., "High-capacity wireless backhaul network using seamless convergence of radio-over-fiber and 90-GHz millimeter-wave," J. Lightw. Technol., vol. 32, no. 20, pp. 3910–3923, Oct. 2014.

[18] P. T. Dat et al., "Full-duplex transmission of LTE-A carrier aggregation signal over a bidirectional seamless fiber-millimeter-wave system," J. Lightw. Technol., vol. 34, no. 2, pp. 691–700, Jan. 2016.

[19] P. T. Dat et al., "High-speed and low-latency front-haul system for heterogeneous wireless networks using seamless fiber-millimeter-wave," in Proc. IEEE Int. Conf. Commun., London, U.K., Jun. 2015, pp. 994–999.

[20] B. L. Dang and I. Niemegeers, "Analysis of IEEE 802.11 in radio over fiber home networks," in Proc. IEEE Conf. Local Comput. Netw., Nov. 2005, pp. 744–747.

[21] K. Kitayama, "Ultimate performance of optical DSB signal-based millimeter-wave fiber-radio system: Effect of laser phase noise," J. Lightw. Technol., vol. 17, no. 10, pp. 1774–1781, Oct. 1999.

[22] J. Beas, "Millimeter-wave frequency radio over fiber systems: A survey," *IEEE Commun. Surv. Tuts.*, vol. 15, no. 4, pp. 1593–1619, Oct.–Dec. 2013.

[23] Y. Tian *et al.*, "60 GHz analog radio-over-fiber fronthaul investigations," *J. Lightw Technol.*, vol. 35, no. 19, pp. 4304–4310, Oct. 2017.

[24] D. Zibar *et al.*, "High-capacity wireless signal generation and demodulation in 75- to 110-GHz band employing all-optical OFDM," *IEEE Photon. Technol. Lett.*, vol. 23, no. 12, pp. 810–812, Jun. 2011.

[25] C.-T. Lin *et al.*, "2 × 2 MIMO radio-over-fiber system at 60 GHz employing frequency domain equalization," *Opt. Express*, vol. 20, no. 1, pp. 562–567, Jan. 2012.

[26] E. P. Martin *et al.*, "25-Gb/s OFDM 60-GHz radio over fiber system based on a gain switched laser," *J. Lightw. Technol.*, vol. 33, no. 8, pp. 1635–1643, Apr. 2015.

[27] X. Li *et al.*, "Long-distance wireless mmwave signal delivery at w-band," *J. Lightw. Technol.*, vol. 34, no. 2, pp. 661–668, Jan. 2016.

[28] A. Kanno *et al.*, "Coherent radio-over-fiber and millimeter-wave radio seamless transmission system for resilient access networks," *IEEE Photon. J.*, vol. 4, no. 6, pp. 2196–2204, Dec. 2012.

[29] J. Zhang *et al.*, "Full-duplex quasi-gapless carrier-aggregation using FBMC in centralized radio-over-fiber heterogeneous networks," *J. Lightw. Technol.*, vol. 35, no. 4, pp. 989–996, Feb. 2017.

[30] U. Gliese, S. Norskov, and T. Nielsen, "Chromatic dispersion in fiberoptic microwave and millimeter-wave links," *IEEE Trans Microw. Theory Techn.*, vol. 44, no. 10, pp. 1716–1724, Oct. 1996.

[31] X. Pang *et al.*, "100 Gbit/s hybrid optical fiber-wireless link in the W-band (75–110 GHz)," *Opt. Express*, vol. 19, no. 25, pp. 24944–24949, 2011.

[32] R. Khayatzadeh *et al.*, "Impact of phase noise in 60-GHz radio-over-fiber communication system based on passively mode-locked laser," *J. Lightw. Technol.*, vol. 32, no. 20, pp. 3529–3535, Oct. 2014.

[33] T. Nagatsuma *et al.*, "Terahertz wireless communications based on photonics technologies," *Opt. Express*, vol. 21, no. 20, pp. 23736–23747, Sep. 2013.

[34] P. T. Dat *et al.*, "190-Gb/s CPRI-equivalent rate fiber-wireless mobile fronthaul for simultaneous transmission of LTE-A and F-OFDM signals," in *Proc. 42nd Eur. Conf. Opt. Commun.*, 2016, pp. 926–928.

[35] G-K. Chang *et al.*, "1–100 GHz microwave photonics link technologies for next-generation WiFi and 5G wireless communications," in *Proc. IEEE Int. Topical Meet. Microw. Photon.*, 2013, pp. 5–8.

[36] P. T. Dat *et al.*, "Simultaneous transmission of multi-RATs and mobile fronthaul in the MMW bands over an IFoF system," presented at the Opt. Fiber Commun. Conf., Los Angeles, CA, USA, 2017, Paper W1C.4.

[37] K. Ikeda *et al.*, "Simultaneous three-band modulation and fiber-optic transmission of 2.5-Gb/s baseband, microwave-, and 60-GHz-band signals on a single wavelength," *J. Lightw. Technol.*, vol. 21, no. 12, pp. 3194–3202, Dec. 2003.

[38] Y.-T. Hsueh *et al.*, "Generation and transport of independent 2.4 GHz (Wi-Fi), 5.8 GHz (WiMAX), and 60-GHz optical millimeter-wave signals on a single wavelength for converged wireless over fiber access networks," presented at the Opt. Fiber Commun. Conf., San Diego, CA, USA, 2009, Paper OTuJ1.

[39] M. Sung *et al.*, "Demonstration of IFoF-based mobile fronthaul in 5G prototype with 28-GHz millimeter wave," *J. Lightw. Technol.*, vol. 36, no. 2, pp. 601–609, Jan. 2018.

[40] L. Giorgi *et al.*, "Subcarrier multiplexing RF plans for analog radio over fiber in heterogeneous networks," *J. Lightw. Technol.*, vol. 34, no. 16, pp. 3859–3866, Aug. 2016.

Pham Tien Dat (M'12) received the B.Eng. degree in electronics and telecommunication engineering from the Posts and Telecommunications Institute of Technology, Hanoi, Vietnam, in 2003, and the M.Sc. and Ph.D. degrees in science of global information and telecommunication studies from Waseda University, Tokyo, Japan, in 2008 and 2011, respectively. In 2011, he joined the National Institute of Information and Communications Technology, Tokyo. His research interests are in the field of microwave/millimeter-wave photonics, radio over fiber, and optical wireless systems.

Atsushi Kanno (M'11) received the B.S., M.S., and Ph.D. degrees in science from the University of Tsukuba, Tsukuba, Japan, in 1999, 2001, and 2005, respectively. In 2005, he was with the Venture Business Laboratory, Institute of Science and Engineering, University of Tsukuba. In 2006, he joined the National Institute of Information and Communications Technology, Tokyo, Japan. His research interests are microwave/millimeter-wave/terahertz photonics, ultrafast optical communication systems, and lithium niobate optical modulators.

Dr. Kanno is a member of the Institute of Electronics, Information and Communication Engineers and the Japan Society of Applied Physics.

Naokatsu Yamamoto received the B.S., M.S., and Ph.D. degrees in electrical engineering from Tokyo Denki University, Tokyo, Japan, in 1995, 1997, and 2000, respectively. From April 2000 to March 2001, he was a Research Associate with Tokyo Denki University. He was also with Tokyo Denki University as a Visiting Associate Professor from May 2008 to June 2012 and the Ministry of Internal Affairs and Communications as a Deputy Director from July 2012 to September 2013. In April 2001, he joined the Communications Research Laboratory (now the National Institute of Information and Communications Technology), Tokyo, where he is currently the Director with the Network Science and Convergence Device Technology Laboratory. He proposed many types of novel crystal growth techniques and successfully developed a quantum dot (QD) optical frequency comb laser, an ultrabroadband QD light source, and a wavelength-tunable QD laser. He demonstrated successfully a high-speed and ultra-broadband photonic transport system constructed with novel nanostructured photonic devices. Recently, he has proposed the use of 1.0-μm waveband photonic transport systems to develop a novel optical frequency resource for optical communications. His research interests include nanostructured materials and III–V semiconductor QD and their photonic device applications in photonic transport systems.

Tetsuya Kawanishi (F'13) received the B.E., M.E., and Ph.D. degrees in electronics from Kyoto University, Kyoto, Japan, in 1992, 1994, and 1997, respectively. From 1994 to 1995, he was with the Production Engineering Laboratory of Panasonic. During 1997, he was with the Venture Business Laboratory, Kyoto University, where he was involved in research on electromagnetic scattering and on near-field optics. In 1998, he joined the Communications Research Laboratory, Ministry of Posts and Telecommunications (now the National Institute of Information and Communications Technology), Tokyo, Japan. During 2004, he was a Visiting Scholar in the Department of Electrical and Computer Engineering, University of California at San Diego. Since April 2015, he has been a Professor with Waseda University, Tokyo. His current research interests include high-speed optical modulators and RF photonics.